Theoretical and Experimental Study of the Thermal Performance of a Multi-use Solar Device

Mohamed H. Ahmed*‡

*Solar Energy Department, National Research Centre, Cairo 12622, Egypt

‡Corresponding Author; Mohamed H. Ahmed, 33 El Buhouth St. Dokki, Tel: +20 100 529 1830,

Fax: +20 237 616 267,mo555as@hotmail.com

Received: 09.06.2018 Accepted:27.07.2018

Abstract- The motivation of building a multi-use solar device is to overcome the disadvantages of single-use devices: solar water heater, dryer, and space heater. Integrating the three devices into one with modifications is the subject of this research to reduce the cost, size, improve the performance, and increase the usage. A thermal model was developed to investigate the performance of the proposed device. Experimental tests were carried out to validate the model. The results show the effects of integrating the water and space heater in the solar dryer performance. The drying air temperature was reduced to reasonable values for drying the agricultural products. The drying temperature was decreased by about 5.1 to 14.1 ºC according to the rate of the hot water consumption for the domestic use and space heating purposes. The weight loss percentage of the dried product (peppermint leaves) had a value of 91.9 % compared to 85.14 % for the single-use dryer. The study shows that the proposed device reduces the cost and size by about 32.4 and 59.7 %, respectively, compared to having three devices. There is a good agreement between the theoretical and experimental results. Consequently, the model can be considered as a valuable tool for researchers.

Keywords Multi-use solar device, Solar dryer, Water heater, Modelling, Cost analysis.

1. Introduction

The use of solar energy in our daily applications has huge advantages: it is a renewable energy, abundantly available, environmentally friendly and it's also free of charge. In spite of these advantages, there are some disadvantages of solar energy devices such as their high cost compared to the traditional devices. Also, the big size of the solar devices still represents an impediment to the spread of solar energy devices. Researchers have long looked for ways to improve the efficiency and cost-effectiveness of solar devices separately. The solar dryer, water heater, space heater, and other solar devices are used to take advantage of solar energy in the daily lives of farmers. Many eminent researchers made several improvements in solar drying technology to meet the desirable drying features [1, 4]. The multi-use solar devices have been studied in many researches to reduce cost and improve performance [5, 7]. Dual purpose solar collector used for heating air and water has been improved using porous matrix below the absorber plate [8]. A hybrid solar dryer was capable of drying at night using stored heat energy collected during the time of sunshine with backup electric heaters located in a water tank [9]. The solar dryer efficiency was raised about 65% by recycling the dryer air. A dual-purpose solar collector (DPSC) was designed to heat air and water simultaneously [10]. The result showed that the system has superior performance to that of dedicated air or water collectors. A new hybrid system which facilitates a dual-purpose solar collector was presented to simultaneously support a dryer system and provide consumptive hot water [11]. In this study, the experiments showed that the system is capable to be used as a domestic drying system as well as providing domestic consumptive hot water. The system would reduce the costs and the required space for installation (about 50%) in comparison with two separate systems for water and air heating. A different configuration of solar combi-systems supplying thermal energy for both domestic hot water and space heating were studied and presented [12]. This study concluded that the optimal solutions depend on the desired objective.

As mentioned above, the design and fabrication of multi-purpose solar devices to convert the solar energy into utilizable energy is vitally important. This study aims to design, construct and test the concept of a multipurpose

(triple-purpose) solar device for agricultural drying, water heating, and space heating. Also, it aims to investigate the continuously hybrid solar dryer by storing the solar energy in a water tank during the daytime and using that energy at night to reduce the drying period and improve the quality of the dried products. The design of a greenhouse solar dryer was modified to work as a solar dryer, water heater, and space heater. A simulation program was developed for the new design of the solar dryer for studying theoretically the effect of the design and the operating parameters on the thermal performance of the multi-purpose solar device. The effect of the hot water flow rate, which represents the heat energy delivered to the space heater or domestic hot water consumption, on the drying performance, was investigated. The Engineering Equation Solver (EES) software was used to solve the governing equations for the proposed solar device. The cost and size reductions were estimated for the multi-purpose device. The following sections present the description of the proposed device, the simulation approach, analysis of the results and the main conclusions.

2. Description of Solar Device

The multi-purpose solar device was designed as a greenhouse solar dryer and modified to work as a water and space heater. The modifications include changing the absorber plate to work as an air and water heater. Circular tubes were welded in the absorber plate so that the water could flow through the tubes. A water storage tank was added to the dryer to store the heated water. An air-water heat exchanger was used to transfer the heat from the storage tank into the dryer chamber at night. Another heat exchanger was installed in a separate room for space warming. Fig. 1 shows three photographs of the multi-purpose solar device installed in the Solar Energy Department, National Research Centre in Cairo, Egypt.

The proposed solar device consists of a wooden chamber insulated from all sides except for the front and the tilted surfaces. The tilted and front surfaces were covered with a single transparent glass cover made of low iron glass, 4 mm in thicknesses. Flat absorber plate made from an iron sheet with 0.4 mm in thickness were black painted and erected under the glass cover, in vertical and tilted positions, to absorb the solar radiation as shown in Fig. 2. Nine circular copper tubes of about 12.5 mm in diameter were attached above the absorber plate by welding. The space between the circular tubes is 9.9 cm. The space between the absorber plate and the glass cover is 12 cm. The angle between the tilted surface and the horizontal was chosen to be 30º which is the optimum angle for the location and research period. The configuration of the absorber plate and the tubes is illustrated in Fig. 3.

A well-insulated cylindrical storage tank with a capacity of 80 l was installed at the top of the dryer. The storage tank was connected to the absorber tubes and the heat exchangers through well-insulated steel pipes. A 150-W circulating fan was installed in the vertical absorber plate to circulate the air from the drying chamber to the channel between the absorber plate and the glass cover. The fan delivers a flow rate of 0.038 m^3/s. A 75 W ventilation fan was installed above the back door of the dryer as shown in Fig. 2. The ventilating air flow rate was 0.018 m^3/s. The air velocity was measured by a calibrated digital hotwire anemometer with an accuracy of ± 0.1 m/s. An air-water heat exchanger with 50 W circulating fan was installed in the bottom of the drying chamber to transfer the heat from the storage tank into the dryer chamber at night or during the absence of solar radiation. A 370 W electric centrifugal pump was used to circulate the hot water from the storage tank to the heat exchanger inside the dryer and the space required to be warmed. The storage tank was prepared also for domestic hot water use. The glass side is oriented due south. The complete configuration of the solar device prototype is illustrated in Fig. 2. The flow of water through the absorber plate, storage tank, dryer heat exchanger, domestic use of hot water, and the space heat exchanger are illustrated in Fig. 3.

Fig. 1. Three photographs of the multi-purpose solar device.

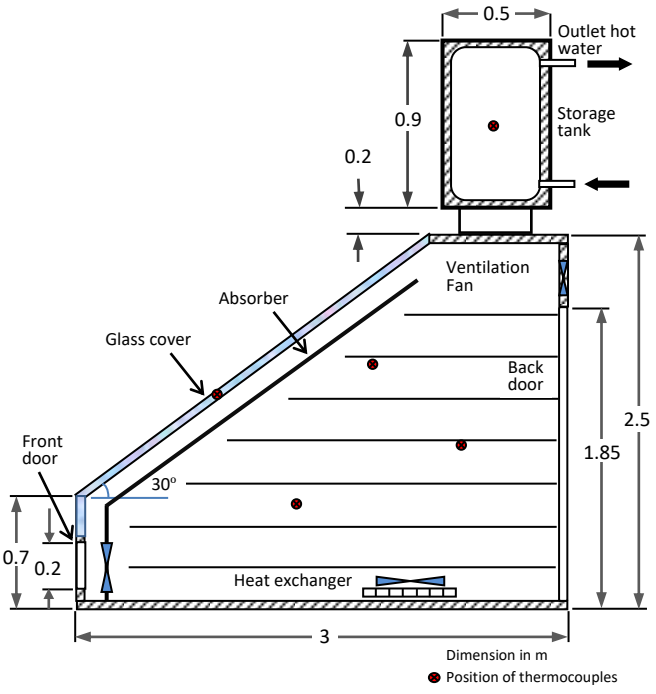

Fig. 2. Side view of the multi-purpose solar device.

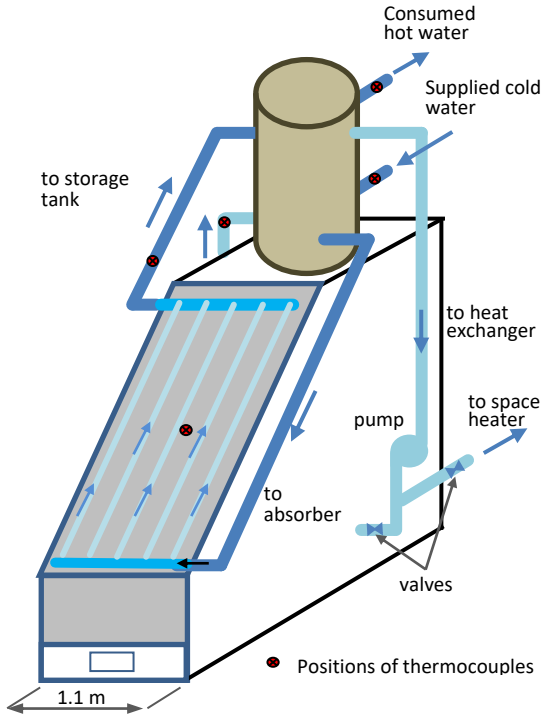

Fig. 3. Schematic diagram for the water flow through the absorber tubes, storage tank, dryer, and space heater.

The solar device prototype was designed to dry 10 kg of fruits or 3 kg of leafy plants. It can also heat 80 l of water from 25 to 59 ºC for domestic use and warm a space of 18 m^3 from 17 to 23 ºC in 27 minutes. Table 1 presents samples of the input parameters for the simulation program.

A 12-channel digital recorder with calibrated copper-constantan thermocouples with an accuracy of ± 0.1 ºC was used to measure the temperature of the crop, absorber plate, air, and water. The positions of the thermocouples are illustrated in Fig. 2 and Fig. 3. A digital moisture content meter was used to measure the moisture content of the crop and the air relative humidity in the dryer with an accuracy of ± 0.1 %. A Kipp and Zonen pyranometer was used to measure the solar intensity on the tilted and front vertical surfaces of the dryer (with a daily uncertainty less than 5%). A digital balance with an accuracy of ± 0.01 g was used to weigh the crop samples at hourly intervals during the drying. The difference in weight between two consecutive reading gives the amount of moisture evaporated during the observed time interval.

In the multi-purpose solar device the absorber plate with the welded tubes absorb the solar radiation and transfer it into heat. The air flows above the below the absorber plate to transfer the heat from the plate to the crops in the dryer trays by convection, some heat can transfer by radiation. The cold water is heated through the welded tubes and flows to the storage tank. The heated water in the storage tank is supplied to a heat exchanger in the bottom of the dryer to transfer its heat to the dryer room at night or at the absent of the solar radiation. The heated water can be also supplied to anther heat exchanger in a separated room to be warmed when required. The heated water can be also used for domestic use.

Table 1. Sample of the input parameters for the simulation program

Input parameter	**Value**	**Unit**
Solar radiation, I_t	0-900	W/m^2
Ambient temperature, T_{amb}	32	ºC
Wind speed, V_w	1.3	m/s
Inlet water temperature, $T_{w,i}$	25	ºC
Water flow rate, $\dot{m}$	0.01	kg/s
Peppermint leaves thickness, s	1.25	mm
Peppermint load	0.5	kg/m^2
Glass transmissivity, α_g	94	%
Glass thickness	4	mm
Absorber plate absorptivity α_{ab}	88	%
Absorber plate thickness	0.4	mm
Area of the tilted absorber plate	3.6	m^2
Area of the front absorber plate	0.4	m^2
Number of available trays	7	trays
Number of tested trays	3	trays
Number of water tubes, n_{tu}	9	tube

3. Thermal Modelling

A one-dimensional theoretical model was built to model the solar radiation incident on the solar collector and absorbed by the receiver plate. The model simulates the heat transfer by convection to the flowing air on both sides of the receiver plate. The heat transfer by radiation from the receiver plate to the glass cover was also simulated as shown in Fig. 4. The heat loss by convection and radiation from the glass cover into the ambient was also simulated. The model calculates the heat energy transfer into the water flow through the tube attached to the receiver plate and the heat transfer from the water fluid into the air of the drying chamber and the space to be heated through the heat exchangers. The following assumptions have been taken for thermal modelling.

- For simplification, the temperature of the absorber plate and the tubes were the same.
- The temperature gradients through the plate and tube thickness were neglected.
- The heat capacity of the dryer walls, fans, and the trays was neglected.
- Thin layer drying has been considered.
- The thermal losses from the tank, the dryer's walls, and the tubes were neglected.

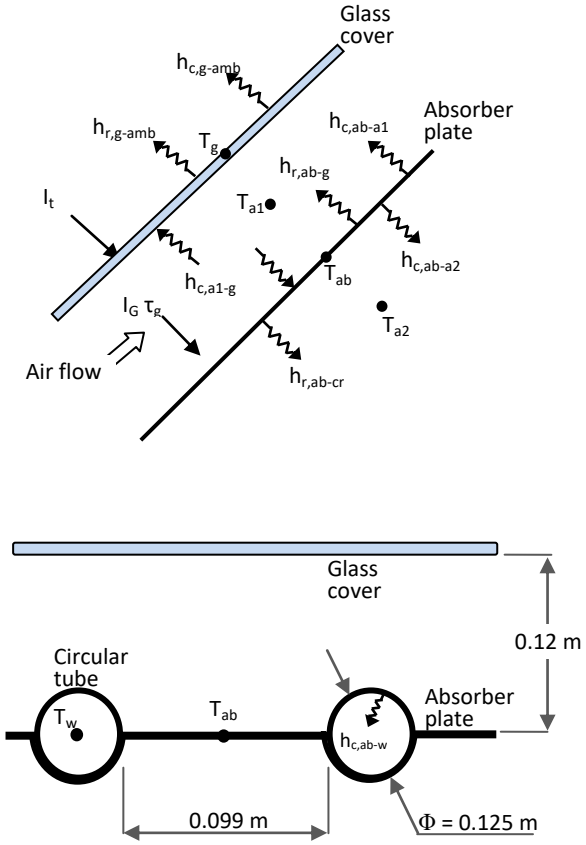

Fig. 4. Model of the heat energy on the glass cover and the absorber plate of the dryer

3.1. Energy Balance for the glass cover.

The energy balance for the glass cover includes the solar energy absorbed by the glass and heat energy transferred to the hot air side and the absorber plate by convection and radiation, respectively in the left terms of Eq. (1). Also, the right terms present the heat losses from the glass cover to the ambient by convection and radiation respectively.

$$I_t\alpha_g + h_{C,a1-g}\left(T_{a1} - T_g\right) + h_{r,ab-g}\left(T_{ab} - T_g\right) = h_{C,g-amb}\left(T_g - T_{amb}\right) + h_{r,g-amb}\left(T_g - T_{amb}\right) \quad (1)$$

Where I_t is the total solar irradiance (W/m^2), α_g is the glass absorptivity, h_C and h_r represents the convective and radiative heat transfer coefficient, respectively. T_{a1} and T_g are the air above the absorber plate and glass cover temperature, respectively.

3.2. Energy Balance for the air flow above the absorber.

The air flow between the absorber plate and the glass cover was symbolled by (a1). The energy balance equation includes the heat gained by the air in the right term of the equation. The left terms include the heat transferred by convection from the absorber plate to the air and from the air to the glass cover respectively as shown in Eq. (2).

$$h_{C,ab-a1}A_{ab}(T_{ab} - T_{a1}) - h_{C,a1-g}A_g(T_{a1} - T_g) = \dot{m}_{a1}Cp_{a1}(T_{a1,i} - T_{a1,o}) \quad (2)$$

Where T_{ab} is the absorber plate temperature, $T_{a1,i}$ is the inlet air temperature, $T_{a1,o}$ is the outlet air temperature, Cp_{a1} is the specific heat of the air above the absorber plate, $\dot{m}_{a1}$ is the air flow rate, A_{ab} and A_g are the area of the absorber plate and the glass cover, respectively.

3.3. Energy balance for the air flow above the absorber.

The energy balance for the absorber plate includes the energy input, which is the solar radiation absorbed by the plate, the energy transferred from the absorber plate to the glass, the air flow above and below the plate and to the water flow through the tubes as shown in Eq. (3).

$$I_tA_{ab}\tau_g\alpha_{ab} = A_{ab}[h_{r,ab-g}(T_{ab} - T_g) + h_{c,ab-a1}(T_{ab} - T_{a1}) + h_{c,ab-a2}(T_{ab} - T_{a2}) + h_{r,ab-cr}\left(T_{ab} - T_{cr}\right)] + h_{c,ab-w}(T_{ab} - T_w)A_{tu}n_{tu} \quad (3)$$

Where τ_g is the glass cover transmissivity, T_{a2} and T_w and are the temperature of the air under the absorber plate and the average water temperature, respectively. T_{cr} is the crop temperature. A_{tu} is the cross-section area of the tube; n_{tu} is the number of the tubes.

3.4. Energy balance for the water flow.

The following equation is the energy balance for water flow through the circular tubes. The right side of the equation represents the heat gained by the water flow. The left side of the equation represents the heat transferred by convection from the absorber plate to the water flow.

$$h_{c,ab-w}\left(T_{ab} - T_w\right)A_{tu}n_{tu} = \dot{m}_w\ Cp_w\left(T_{w,i} - T_{w,o}\right) \quad (4)$$

Where $T_{w,i}$ and $T_{w,o}$ are the inlet and outlet water temperature, $\dot{m}_w$ is the water mass flow rate and Cp_w is the specific heat of the water.

3.5. Energy balance for the air under the absorber.

The energy balance for the air flow below the absorber plate is presented in Eq. (5). The left terms include the heat transfer by convection from the absorber plate to the air and from the air to the crop. The right term of the equation presents the heat gained by the air flow.

$$h_{C,ab-a2}A_{ab}(T_{ab} - T_{a2}) - h_{C,a2-cr}A_{cr}\left(T_{a2} - T_{cr}\right) = \dot{m}_{a2}Cp_{a2}\left(T_{a2,i} - T_{a2,o}\right) \quad (5)$$

3.6. Energy balance for the crop.

The right term of the following equation represents the evaporation energy gained by crop, and the parcels in the left side are the heat input by convection and radiation and the evaporative heat losses, respectively.

$$h_{c,a2-cr}A_{cr}\left(T_{a2}-T_{cr}\right)+h_{r,ab-cr}A_{ab}\left(T_{ab}-T_{cr}\right)=L\ m_w \quad (6)$$

Where A_{cr} is the surface area of the cope, L is the latent heat of vaporization, m_w is the water mass in the crop.

The energy balance equations for all items were solved simultaneously every 0.5 hour due to the change of solar irradiance through the day.

3.7. Governing equation of drying process.

The larger portion of the energy consumed during drying is for transforming liquid water into vapour. Peppermint leaves were selected as a sample crop. The modelling of peppermint leaves was considered as a thin layer drying process [13]. The moisture ratio (MR) of peppermint leaves was given by Eq. (7):

$$MR=\frac{M-M_e}{M_i-M_e} \quad (7)$$

Where M is the moisture content at any time; M_i and M_e are the initial and the equilibrium moisture content, respectively. M_e is very small in comparison to M_i and M, hence M_e can be neglected and the moisture ratio can be presented in a simplified form as follow [14]:

$$MR=\frac{M}{M_i} \quad (8)$$

The drying data of peppermint leaves were fitted into three empirical thin-layer drying models as shown in Table 2, which are widely employed for determining the drying curves.

Table 2. Appearance properties of accepted manuscripts

Model number	Model name	Model equation	References
1	Newton	MR= exp(–kt)	[15]
2	Henderson and Pabis	MR= a exp(-kt)	[16]
3	Logarithmic	MR=a exp(–kt)+c	[17]

Fick's second law is used to describe the drying rate behavior of any material in the falling rate drying period [18].

$$\frac{\partial M}{\partial t}=D_v\nabla^2\ M \quad (9)$$

Where D_v is the effective mass diffusivity, t is time, and ∇ is the one-dimensional Nabla squared operator. The solution of Fick's second law in slab geometry after simplification, with the assumptions of moisture migration being by diffusion, was as follows [10]:

$$MR=\frac{8}{\pi^2}\exp\left(\frac{-\pi^2 D_v t}{4s^2}\right) \quad (10)$$

The dimensionless weight loss W_{loss} of drying material is calculated using the following equation:

$$W_{loss}=\frac{W_t-W_i}{W_i} \quad (11)$$

Where W_i is the initial weight of peppermint, W_t weight at any time.

3.8. The device efficiency.

The instantaneous efficiency η of the multi-use device is the heat gained by the air divided by the incident solar radiation on the collector surface area AC and can be calculated from the following equation:

$$\eta=\frac{\dot{m}_a\ Cp_a\ \Delta T_a}{I_t\ A_c} \quad (12)$$

Where ΔT_a is the air temperature difference. The previous equations were solved using EES software to predict the temperature of the glass cover, absorber plate, air flow between the glass and the absorber, and the airflow under the absorber. Also, the moisture content and weight loss of the peppermint leaves were calculated versus time.

3.9. Validation method of the theoretical results.

The correlation coefficient (r) and root mean square percent deviation (e) have been calculated to compare the theoretical with the experimental results. The correlation coefficient is probably the most commonly reported statistic in method comparison studies. It simply represents the ratio of variation between the predicted and measured values. While the root mean square percent deviation (e) is used because it's good measure of errors. It also measures the quality of the models and also the predictability power of the model. It is differentiable, so it is easy to calculate or compute the solution. It is symmetric and quadratic, which is suitable for Gaussian noises. It's useful for showing bigger deviations. By squaring the errors we can get more accurate results as the negative and positive errors don't cancel out each other and stay in existence, thus adding more accuracy to the result. The following equations were used to evaluate these parameters [19].

$$r=\frac{N\sum X_i\ Y_i-\sum X_i\ \sum Y_i}{\sqrt{N\sum\left(X_i\right)^2-\left(\sum X_i\right)^2}\ \sqrt{N\sum\left(Y_i\right)^2-\left(\sum Y_i\right)^2}} \quad (13)$$

Where X_i is the theoretical value of a parameter, Y_i is the experimental value of a parameter, and N is the number of values.

$$e=\sqrt{\frac{\sum\left(e_i\right)^2}{N}} \quad (14)$$

$$\text{Where } (e_i)=\left[\frac{X_i-Y_i}{X_i}\right]\times 100$$

This indicates the percentage deviation of the experimental values of parameters from the theoretical values.

4. Thermal Modelling

In this study, the performance of the multi-purpose solar device was investigated for solar drying, solar water heating and space heating. The effect of the hot water consumption for domestic use on the drying process was also investigated. The experiments were carried out for drying the peppermint at hot water consumption of 0, 1, 5 and 10 l/h. The quantity of the peppermint used in each drying cycle was 3 kg. The peppermint leaves were put on shelves of plastic mesh with a bulk thickness ranging from 5 to 10 cm. After completing the drying process, the reduction in thickness ranges from 1.5 to 2.5 cm.

The ambient temperature and the solar irradiance incident on the tilted and vertical surfaces for the location of the experiments at the middle of June are shown in Fig. 5. Fig. 6 presents, theoretically and experimentally, the variation of W_{loss} with time at different consumption rates of hot water from the storage tank for cases. The obtained W_{loss} percentages were 88.4, 86.9, 84.1 and 78.8 % after eleven hours for the peppermint at water consumption rates of 0, 1, 5, and 10 l/h respectively. Increasing the water consumption decreased the W_{loss} due to decreased absorber plate temperature and consequently the air temperature above the product. According to the figure, the product weight loss was high initially and reduced with time. The theoretical results were validated with the experimental results and the verification proved that the results were identical and significantly similar. The figure shows good agreement between the experimental and the theoretical results where the correlation coefficient value (r) fluctuates around the value of 0.98 and the root mean square percent deviation (e) fluctuates around the value of 4.01 for all curves in the figure.

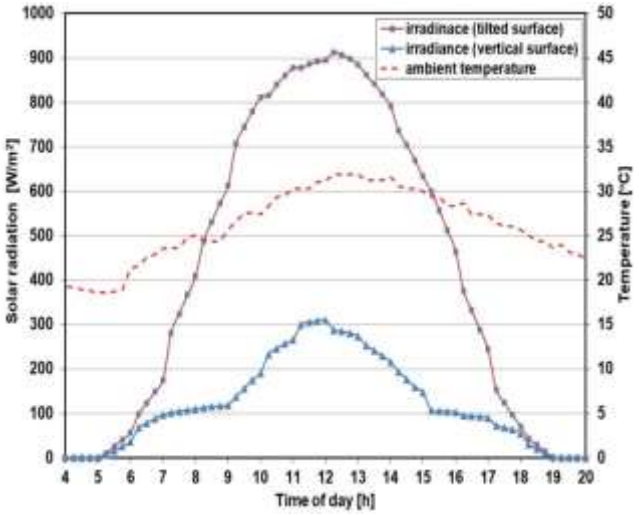

Fig. 5. The ambient temperature and the total solar radiation on the tilted and vertical surfaces.

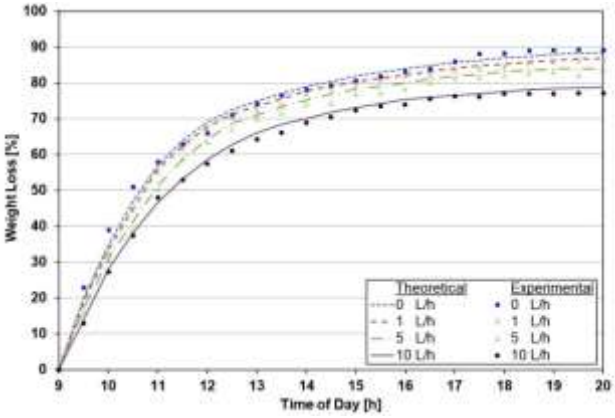

Fig. 6. The theoretical and experimental validation for the weight loss percentage variation of the peppermint.

Fig. 7 presents the drying air temperature inside the drying chamber at hot water consumption rates of 0, 1, 5, and 10 l/h for domestic use. From the figure, it can be seen that the air temperature decrease by significant values with increasing the water consumption rate to 5 and 10 l/h. At solar noon, the decrease in the drying air temperature ranges from 5 to 13 ºC with increasing the water rate consumption to 5 and 10 l/h respectively. The decrease in the drying air temperature is very small (from 1 to 2 ºC) at a hot water flow rate of 1 l/h. The figure shows a fair agreement between the theoretical and experimental data. The correlation coefficient (r) fluctuates around 0.98 and the root mean square percent deviation (e) fluctuates around 3.29 for all curves.

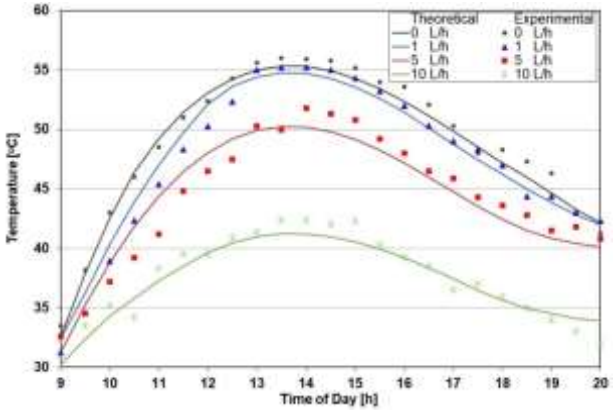

Fig. 7. The theoretical and experimental drying air temperature at different hot water consumptions.

The measured and calculated values of the outlet water temperature from the absorber, air temperature, and the average hot water temperature in the storage tank are presented in Fig. 8 at 5 l/h hot water consumption. In the early morning, due to the low solar radiation, the outlet water temperature and the average tank temperature are low and increases with increasing solar radiation. There are differences between the outlet water temperature and the average temperature due to the low water temperature at the bottom of the tank. With the progress of time, the tank bottom temperature increases when there is no hot water consumption. The water tank temperature approaches the outlet water temperature after solar noon. The air inside the drying chamber has the same profile as the outlet water temperature.

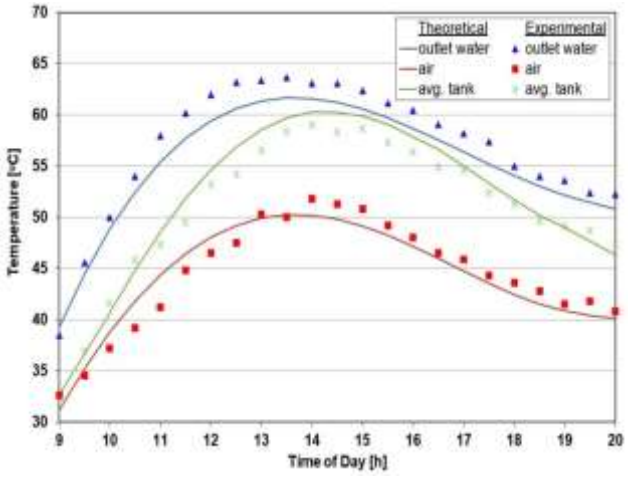

Fig. 8. The outlet water temperature, air temperature, and the average water tank temperature.

Fig. 9 presents the calculated and measured air temperature delivered to the drying chamber in single-use (as dryer) and multi-use (as a dryer, water heater, and a space heater). In the multi-use case, the hot water consumptions were 5 l/h and 10 l/h while in the single-use cases there was no hot water consumption. For the single use case, the drying air temperature varied through the day and reached a maximum value of 55.3 ºC, while in the multi-use case, the drying air reached a maximum value of 50.2 and 41.2 ºC for hot water consumption rates of 5 and 10 l/h, respectively. The percentage difference between the calculated and measured values of the air temperature in the single and multi-use cases ranged from -4.38 to 6.27 %. In case of multi-use, the reductions in the air temperature were 5.1 and 14.1 ºC corresponding to hot water consumption of 5 and 10 l/h at solar noon, respectively. From the figure, it is clear that the consumption of 10 l/h of hot water leads to a big reduction in the drying air temperature while for consumption of 5 l/h the reduction is reasonable and enough to complete the drying process.

During the solar drying process in a greenhouse dryer, air ventilation is required to control the humidity and the air

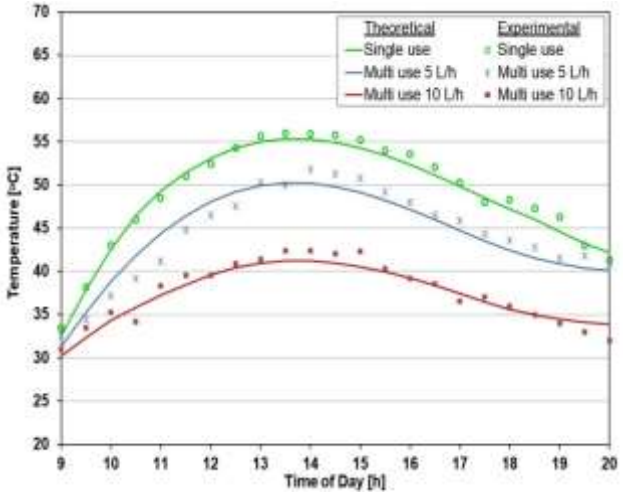

Fig. 9. The drying air temperature at single and multi-use cases of the multi-purpose solar device.

temperature inside the dryer to prevent the overheating inside the drying chamber. Part of the heat energy comes out with the ventilated air. In the multi-use solar device, the excess part of the heat is extracted through the flow of water in the tubes. The heat extracted is stored in a storage tank to be used during insufficient solar radiation. An air-water heat exchanger is used to supply heat energy from the storage tank to the drying chamber during the low solar radiation. Fig. 10 presents the percentage weight loss of the dried product with and without using the heat exchanger. The Figure shows the enhancement in the weight loss percentage due to using the stored heat energy through the heat exchanger. From the figure, it can be clearly seen that the weight loss percentages were initially high and then decreased. We can also observe a continuous reduction in weight loss percentage after sunset due to using the heat exchanger. The weight loss percentage increased to 91.9 % using the air-water heat exchanger compared to 88.4 % in the case of no heat exchanger.

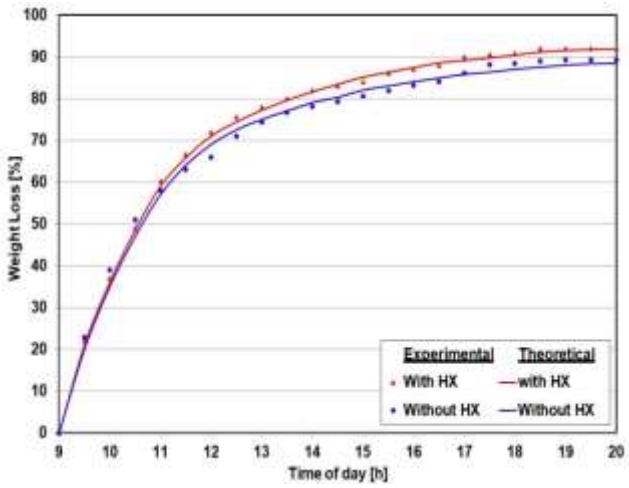

Fig. 10. Theoretical and experimental percentage weight loss of peppermint.

Agreement between the simulation and experimental results was observed in the first period of the drying process. In the second period, the experimental results started to deviate from the theoretical data as a result of some assumptions that were not fully identical to reality, such as the homogeneity of solar radiation along the absorber surface and accumulating some dust on the glass surface. However, this deviation is still acceptable since it is not more than 1.6 % at its worst.

The daily useful energy gained from the multi-use device and each separated device were calculated using the simulation program for all months of the year regardless of the actual operating periods of each device. Fig. 11 presents the daily energy gained from all devices. From the figure, it can be observed that the daily energy gained from the multi-use device is higher than the energy gained from the solar water heater, solar dryer, and the solar space heater. The daily energy gained from the multi-use device varied from 6.6 to 17.5 MJ/m^2.

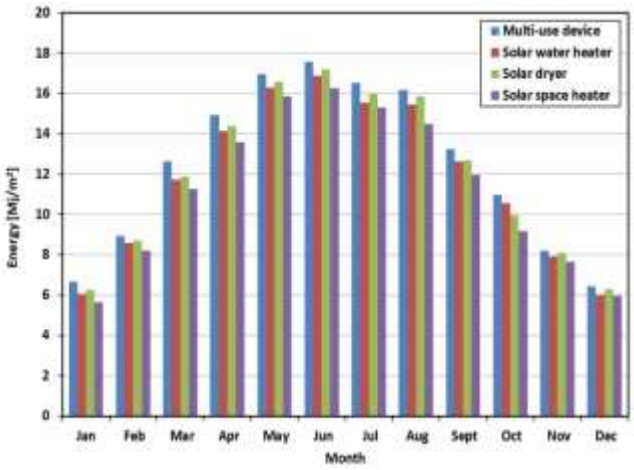

Fig. 11. The daily energy gained from the multi-use device and the three single solar devices

For the cost analysis, a detailed cost evaluation of the multi-purpose solar devices was considered and compared with the cost of three individual solar devices (solar dryer, water heater, and a space heater) as shown in Table 3. The multi-use solar device was evaluated to dry 10 kg of fruits or 3 kg of leafy plants, heats 80 l of water and warms a space of 18 m^3 from 17 to 23 ºC.

Table 3. The cost of the multi-use solar device and the three single solar devices

Item	Multi-use device L.E.	Water heater L.E.	Solar dryer L.E.	Space heater L.E.
Drying chamber	3800	-	3800	-
Insulating box	-	1600	-	1900
Absorber plate	130	180	220	220
Fluid tubes	900	900	-	-
Fans	660	-	440	220
Connecting tubes	260	140	-	-
Pump	450	-	-	-
Storage tank	3000	3000	-	-
Heat exchanger	250	-	-	250
Manufacturing	3200	1800	2250	1800
Sum	**12650**	**4620**	**6690**	**4390**
		18700		

From table 3, we can observe that the total cost of the multi-use solar device and three separated single-use devices are 12650 and 18700 L.E. (Egyptian Pound), respectively. This means that the cost reduction due to using the multi-use device is 6050 L.E which represents 32.4 %. The cost comparison doesn't take the total output heat from the three single devices as a base of comparison. The comparison assumes that every single device will operate in a different seasonal period and not at the same time. Table 4 presents a comparison between the rate of energy gained from the proposed device and the three single-use devices at solar noon.

Table 4. The maximum efficiency and rate of energy gained from the solar devices.

Item	Multi-use device	Water heater	Solar dryer	Space heater
Absorber area, m^2	4	3.6	4	3.6
Device efficiency, %	71	68	65	66
Rate of energy gained, kW	2556	2203	2340	2138

From tables 3 and 4, we can conclude that the proposed multi-purpose device is a better choice than the three single-use devices if these devices operate at different times and not simultaneously. The total space required for the multi-use device and the three single devices are 12.2 m^3 and 30.3 m^3, respectively. Consequently, the reduction in the required space is 18.1 m^3 which is 59.7 %. So we can conclude that the multi-use solar device solved the problems of the high cost and the big size of the solar application devices. Where, the reductions in the cost and size are 32.4 % and 59.7%, respectively.

5. Conclusion

The thermal performance of a multi-use solar device was studied numerically and the results were validated experimentally. The numerical investigation of the multi-use solar device was performed using the ESS software. The performance of the solar device was investigated when it worked only as a solar dryer and as a multi-use solar device. The effects of operating the device as a solar water heater and a space heater beside the solar dryer were represented by the quantity of the hot water consumption from the storage tank which reflects the quantity of water flow rate through the circular tube. Increasing the water consumption rates from 0 to 10 l/h decreased the weight loss percentage of the crop from 88.4 to 78.8 %. Consequently, the moisture content in the product increased from 0.025 to 0.259 kg H_2O/kg dry matter. The drying performance was reduced with increasing the water flow rate of the water and space heater.

By using the air-water heat exchanger, the weight loss percentage of the dried product was reduced to 8.3 % compared to 14.1 % in the case of not using the heat exchanger. The reduction in the outlet water temperatures due to using the proposed device was 6.3 and 4.2 ºC at solar noon and in the morning and evening, respectively compared to the single solar water heater device. The reduction in the total cost and size of the multi-use solar device are 6050 L.E (32.4%) and 18.1 m^3 (59.7 %), respectively. The results show a great similarity between the experimental and theoretical

results. The simulation program can be considered as a valuable simulation tool for researchers and engineers.

Acknowledgements

The author gratefully acknowledges the support and fund given by National Research Centre NRC through the 10th In-house Research Projects.

References

[1] P. Barnwal, G. N. Tiwari, "Grape drying by using hybrid photovoltaic–thermal (PV/T) greenhouse dryer: an experimental study", Solar Energy, Vol. 82, pp. 1131-1144, 2008.

[2] A. Aziz, S. U. Rehman, S. U. Rehman, "Exergy Analysis of Solar Cabinet Dryer and Evaluate the Performance Enhancement of Solar Cabinet Dryer by Addition of Solar Reflectors", International Journal of Renewable Energy Research, Vol. 6, No. 4, pp. 1396-1402, 2016.

[3] D. Parikh, G. D. Agrawal, "Solar Drying In Hot and Dry Climate of Jaipur, India", International Journal of Renewable Energy Research, Vol. 1, No. 4, pp. 224-231, 2011.

[4] V. Ermuratskii, V. Oleschuk, F. Blaabjerg, "Experimental Investigation of Two Modified Energy-Saving Constructions of Solar Greenhouses", 4th International Conference on Renewable Energy Research and Applications (ICRERA 2015), Palermo, Italy, pp. 339-342, 22-25 Nov. 2015.

[5] S. Bezari, A. Bekkouche, H. Bensaha, A. Benchatti, "Amelioration of a greenhouse through energy storage system Case study: Ghardaia region (Algeria)", 4th International Conference on Renewable Energy Research and Applications (ICRERA 2015), Palermo, Italy, pp. 578-582, 22-25 Nov. 2015.

[6] M. E. Toygar, O. Incesu, Z. Cetin, T. Bayram, A. Toygar, "SOLARUX CSP greenhouse, cultivates agricultural products, generates electrical energy, industrial fruit and vegetables drying with wasted heat energy", 6th International Conference on Renewable Energy Research and Applications (ICRERA 2017), San Diego, USA, pp. 198-194, 5-8 Nov. 2017.

[7] E. M. Toygar, T. Bayram, O. Das, A. Demir, E. T. Turkmen, "The development and design of Solarux system with solar flat mirror and solid material high-temperature heat storage", 2nd International Conference on Renewable Energy Research and Applications (ICRERA 2013), Madrid, Spain, pp. 458-463, 20-23 Oct. 2013.

[8] A. Venu, P. Arun, "Simulation Studies on Porous Medium Integrated Dual Purpose Solar Collector", International Journal of Renewable Energy Research, Vol. 3, No.1, pp. 114–120, 2013.

[9] B. Amer, M. Hossain, K. Gottschalk, "Design and performance evaluation of a new hybrid solar dryer for banana", Energy Convers. Manage, Vol. 51, pp. 813-820, 2010.

[10] M. R. Assari, H. B. Tabrizi, I. Jafari, "Experimental and theoretical investigation of dual purpose solar collector", Solar Energy, Vol. 85, pp. 601-608, 2011.

[11] A. Mohajer, O. Nematollahi, M. M. Joybari, S. A. Hashemi, M. R. Assari, "Experimental investigation of a Hybrid Solar Drier and Water Heater System", Energy Convers. Manage., Vol. 76, pp. 935-944, 2013.

[12] A. Rey, R. Zmeureanu, "Multi-objective optimization framework for the selection of configuration and equipment sizing of solar thermal combisystems", Energy, Vol. 145, pp. 182-194, 2018.

[13] I. Doymaz, "Thin-layer drying behavior of mint leaves", J. Food Eng. Vol. 74, pp. 370-375. 2006.

[14] R. K. Goyal, A. R. P. Kingsly, M. R. Manikanthan, S. M. Ilyas, "Mathematical modeling of thin layer drying kinetics of plum in a tunnel dryer", J. Food Eng., Vol. 79, pp. 176-180, 2007.

[15] A. Akbulut, A. Durmus, "Thin layer solar drying and mathematical modeling of mulberry", Int. J. Energy Res., Vol. 33, pp. 687-695, 2009.

[16] D. O. Arslan, M. M. Zcan, H. O. Menges, "Evaluation of drying methods with respect to drying parameters, some nutritional and colour characteristics of peppermint (Mentha x Piperita L.)", Energy Convers. Manage, Vol. 51, pp. 2769-7275, 2010.

[17] A. Midilli, H. Kucuk, "Mathematical modeling of thin layer drying of pistachio by using solar energy", Energy Convers. Manage, Vol. 44, pp. 1111-1122, 2003.

[18] M. X. Ng, T. C. Tham, S. P. Ong, C. L. Law, "Drying kinetics of technical specified rubber", Inf Process Agric., Vol. 2, pp. 64-71, 2015.

[19] G. N. Tiwari, R. K. Mishra, Advance Renewable Energy Sources, RSC publishing, 2012.